JOURNAL OF GEOPHYSICAL RESEARCH, VOL. 96, NO. C12, PAGES 22,135–22,150, DECEMBER 15, 1991

Seasonal and Interannual Variations of Sea Surface Salinity in the Tropical Pacific Ocean

THIERRY DELCROIX AND CHRISTIAN HÉNIN

Groupe SURTROPAC, Institut Français de Recherche Scientifique et Technique Pour le Développement en Coopération (ORSTOM), Nouméa, New Caledonia

Sea surface bucket measurements, obtained through a ship-of-opportunity program, are used to describe the sea surface salinity (SSS) field for the tropical Pacific during the period 1969–1988. Emphasis is placed upon the mean SSS distribution and the seasonal and interannual SSS variability occurring along four well-sampled shipping tracks. These tracks extend from New Zealand to Japan, from New Zealand to Hawaii, from Tahiti to California, and from Tahiti to Panama. They cross the equator at 155°E, 160°W, 140°W, and 100°W, respectively. Along each track, the mean SSS distribution is characterized by SSS minima which are 4°–6° further poleward than the axes of maximum precipitation associated with the Intertropical Convergence Zone (ITCZ) and South Pacific Convergence Zone (SPCZ). It is suggested that these SSS minima owe their existence mainly to heavy rainfall and poleward Ekman salt transport associated with the trade winds. The role of zonal salt advection was found negligible for these SSS minima. Except along the eastern track, maximum seasonal SSS variations are located in the ITCZ and SPCZ regions, with minimum SSS in September–October and March–April, respectively. On the basis of precipitation island stations, it is demonstrated that the maximum seasonal SSS variations are closely related to the rainfall regimes of the ITCZ and SPCZ (rainfall maximum 3 months before SSS minimum; rainfall amount sufficient to account for SSS changes). Along the eastern track, a strong annual SSS cycle is found from about 4°S (110°W) to the Panama coast (minimum SSS in February–March), reflecting the combined effects of rainfall, salt advection, and vertical mixing. Notable interannual SSS variability concerns only the western half of the tropical Pacific Ocean where El Niño–Southern Oscillation (ENSO) related SSS changes are strongly related to ENSO-related precipitation changes. During ENSO periods, the SSS field west of about 150°W is characterized by fresher-than-average SSS within about 8°N to 8°S, and conversely saltier-than-average SSS poleward of 8° latitudes. These modifications in the SSS field are thought to result mainly from an eastward displacement in the ascending branch of the Walker and Hadley cells which induces unusually high rainfall over the western and central equatorial Pacific region bordered on all sides by rainfall deficits. Reproducing the actual SSS changes at seasonal and interannual time scales would be a very stringent test for model capability.

1. INTRODUCTION

The distribution of salt in the world ocean and its seasonal and interannual variability are important in understanding the role of the ocean in the Earth's climate. Salt has a dynamic role in the thermohaline circulation and thus in the related distribution of mass and heat [e.g., *Bryan*, 1986]. Salinity can also control the formation of water masses, and it can be used for circulation tracer studies [*Sverdrup et al.*, 1942]. Salinity is further of thermodynamic importance. The salinity stratification is known to affect the depth of penetrative convection at high latitudes [e.g., *Lazier*, 1982], and it may also determine the mixed-layer depth in equatorial regions [*Lukas and Lindstrom*, 1991]. In tropical regions, salinity is useful too as an indicator of precipitation and evaporation [*Donguy and Hénin*, 1976*a*]. Generally speaking, salinity is of major interest in studies of surface water fluxes. In addition, salinity distribution is important for determining the equation of state of the ocean and, in particular, for the computation of dynamic height anomalies. In this context, knowledge of sea surface salinity (SSS) can be of great help in improving estimates of dynamic height anomalies obtained from temperature profiles and mean temperature-salinity (*T-S*) curves [*Kessler and Taft*, 1987]. Knowledge of dynamic height variations is necessary for computing geostrophic circulation, and evaluating satellite altimetric measurements. Finally, the salinity field needs to be included in numerical models to perform accurate simulation of tropical oceans [*Miller*, 1976; *Cooper*, 1988].

Since salinity data are so vital in tropical oceanographic and meteorological studies, it may appear surprising that very little information exists about salinity variations in the tropical oceans. Indeed, a three-dimensional salinity field only relies on hydrocast and CTD (conductivity-temperature-depth) (CTD) measurements which are rather sparse, particularly for the huge tropical Pacific ocean. For this reason, most investigators have only analyzed the more numerous surface salinity measurements using observations from research cruises and/or from ship-of-opportunity (SOP) programs.

On the basis of research cruises, *Reid* [1969] presented maps of sea surface salinity for the Pacific Ocean in summer and in winter. *Neumann* [1969] found a close inverse correlation between the seasonal variations of local rainfall and surface salinity off the coast of Brazil between the Amazon River estuary and 10°S. *Donguy and Hénin* [1976*b*] analyzed the influence of the 1957–1958 and 1972–1973 El Niño events upon SSS distribution over the tropical Pacific Ocean (150°E to 130°W, 10°N to 25°S). *Donguy and Hénin* [1978] noted a relation between time variation of SSS along the 180° meridian (22°S to 8°N) and rainfall at nearby island stations. Furthermore, they found higher SSS around the equator, which they attributed to equatorial upwelling. *Levitus* [1986] described the annual cycle of SSS in the world ocean from a

Paper number 91JC02124.
0148-0227/91/91JC-02124$05.00

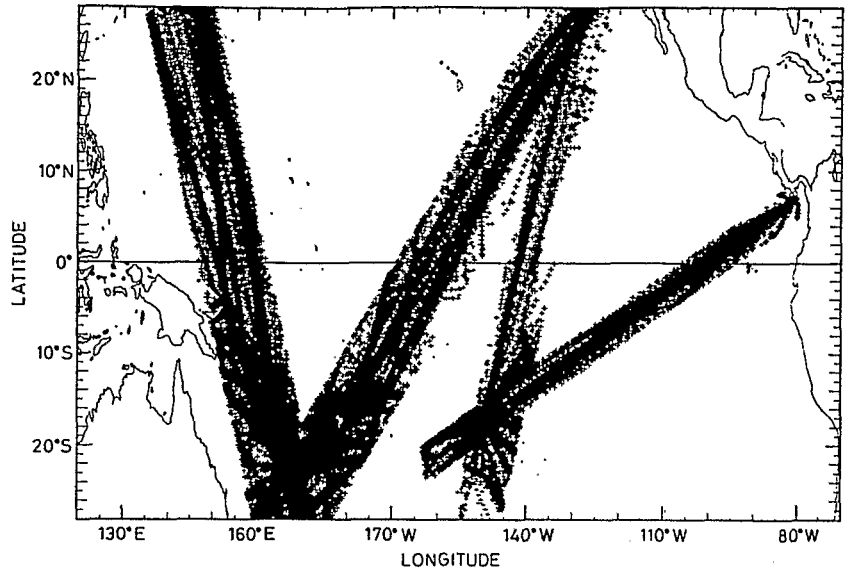

Fig. 1. Spatial distribution of the sea surface salinity data collected along four mean shipping tracks in the tropical Pacific for the period 1969–1988. From west to east, these tracks are referred to as the western track, the central track, the east central track, and the eastern track throughout the paper.

composite of an unprecedently large numbers of observations that, however, are still poorly distributed in space and time.

The aforementioned SSS studies, based on hydrological data, clearly did not have the time-space continuity required to identify seasonal and interannual salinity variations. This continuity has been partly achieved for surface measurements, using merchant ships. *Hires and Montgomery* [1972] analyzed the 1957–1965 SSS changes along a track from Samoa to Hawaii. They reported that a comparison between annual variations of SSS and precipitation was "inconclusive." *Donguy and Hénin* [1975, 1977] studied SSS changes along the New Caledonia to Japan shipping track. They suggested that the 5°–12°S and 7°–15°N SSS minima, observed during February–June and July–December, respectively, are due to local precipitation associated with the convergence zones of the wind. Along the same track, *Donguy and Dessier* [1983] found that the 1974–1982 SSS changes, within 6°N to 10°S, were mostly related to the moderate 1976–1977 and aborted 1979–1980 El Nino events. Variations of SSS between Tahiti and Panama, from mid-1974 to the end of 1978, were analyzed by *Donguy and Hénin* [1980]. *Saur* [1980] studied annual and interannual SSS variability using 8.5 years of observations between San Francisco and Hawaii. In the southwestern tropical Pacific, *Delcroix and Hénin* [1989] demonstrated that seasonal and interannual variations of SSS are consistent with the rainfall regime associated with the meridional migration of the South Pacific Convergence Zone (SPCZ). Recently, *Delcroix and Masia* [1989] presented an atlas of monthly SSS changes along four trans-Pacific shipping tracks for the period 1969–1988.

The present paper aims to describe the seasonal and interannual variability of SSS along the shipping tracks defined in the atlas of *Delcroix and Masia* [1989]. These tracks extend roughly from New Zealand to Japan, from New Zealand to Hawaii, from Tahiti to California, and from Tahiti to Panama (Figure 1). Some of the along-track SSS data have already been used in the literature (see the references of *Donguy* [1987]). Hence some of the previous results will be updated and confirmed in the present paper, but with the addition of 10 years of SSS measurements including the ones obtained during the 1982–1983 and 1986–1987 El Nino events.

The paper is organized as follows. Section 2 presents the along-track SSS data sets, their processing and gridding, and the expected errors of the SSS values. Section 3 briefly outlines the equation for sea surface salinity changes to establish the framework of our analysis. The mean distributions and the mean seasonal cycles of SSS are discussed in sections 4 and 5, respectively. The interannual variability in SSS is then tackled in section 6 through an empirical orthogonal function (EOF) analysis which will unambiguously stress El Niño effects upon SSS changes in the western half of the tropical Pacific. Conclusions appear in section 7.

2. DATA AND DATA PROCESSING

The bulk of this work is based on SSS measurements obtained through an ORSTOM (Institut Français de Recherche Scientifique et Technique Pour le Développement en Coopération) SOP operated from Nouméa (New Caledonia) and Papeete (Tahiti, French Polynesia) since 1969 and 1976, respectively. SSS measurements were obtained from water samples bottled by ship officers every 30–60 n. mi. (55–110 km) and later analyzed on shore by laboratory salinometers.

During the period 1969–1988 the ORSTOM SOP collected 135,000 water samples for the tropical Pacific (30°N to 30°S). From these, we have selected about 102,000 observations situated along the four well-sampled shipping tracks shown in Figure 1. Details about time-space distributions of SSS along each track are given by *Delcroix and Masia* [1989]. For brevity, these tracks will be referred to as the western track (166°E, 28°S, to 142°E, 28°N), the central track (166°E, 28°S, to 126°W, 28°N), the east central track (152°W, 28°S to 126°W, 28°N), and the eastern track (152°W, 22°S, to 80°W,

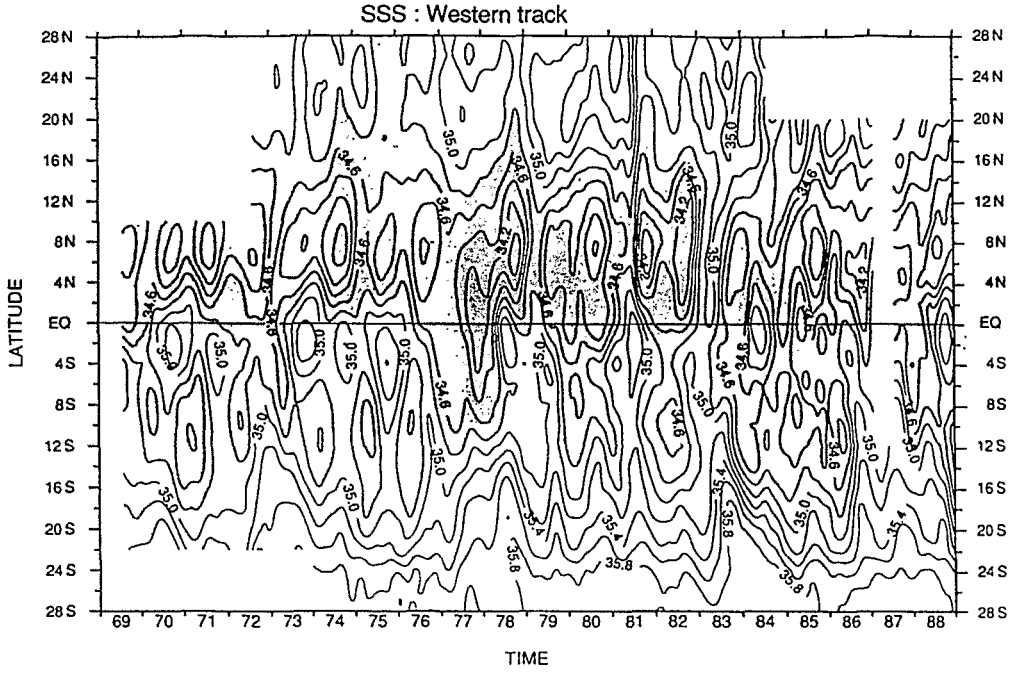

Fig. 2. Time-latitude diagram of sea surface salinity for the western track. Contour intervals are 0.2, and shaded areas denote sea surface salinity below 34.8.

7°N). The tracks cross the equator at 155°E (1000 km wide), 160°W (1000 km wide), 140°W (775 km wide), and 100°W (445 km wide), respectively. For the western, central, east central, and eastern tracks, we analyze SSS data from 1969–1988, 1975–1988, 1976–1988, and 1974–1988, respectively.

Measurements of SSS were routinely checked before being entered into the ORSTOM data base. Preliminary quality assurance was handled through procedures that checked for internal consistency and climatic limits. For each transit, geographic position and SSS value of each sample were reported on a map in order to detect position errors and dubious measurements. Then, for tropical regions, a basic test systematically rejected SSS values greater than 37 or smaller than 30 psu. Additional validation tests were applied to our selected SSS values. Along each track, spurious SSS measurements were detected through objective criteria based on multiples (±5, ±4, and then ±3.5) of sample standard deviations computed in 2° latitude bands. The resulting assumed spurious measurements (0.5%) were rejected.

Irregularly distributed along-track SSS data were then gridded onto regular grid meshes by an objective interpolation scheme (Laplacian method: $\nabla^2 S = 0$). The grid element size was 2° latitude (e.g., 1°N to 1°S) and 1 month. It was chosen to be large enough to include a sufficient number of SSS measurements so that a gridded SSS value is a meaningful quantity. Such a grid size restricts our investigation to obvious time and space scales. On a mean, a grid element represents 9.6, 6.6, 2.4, and 5.7 measurements of SSS, from the western to the eastern tracks. The gridded SSS values were then smoothed in the time-latitude domain (Laplacian smoothing: $S_{\text{smoothed}} = S + 1/16\ \nabla^2 S$), and a $\frac{1}{4}, \frac{1}{2}, \frac{1}{4}$ filter was applied on each time series to reduce remaining small-scale noise. The time-latitude matrix of the resulting processed SSS are graphically presented in Figures 2 to 5.

Before analyzing the processed along-track SSS data, it is necessary to assess the expected accuracy of these data. As was mentioned previously, the raw SSS values were derived from water samples. Most of these were collected by bucket, except along the western track where about 25% of the 1969–1972 samples were obtained from main ship seawater systems. In these latter cases, observations are more representative of the water between 4 and 8 m, depending on the ship and load. These intake measurements, representing roughly 2% of the analyzed data, were not disregarded in our analysis because they are not detectable in our data base. When they happen to be present, one should keep in mind that they may slightly bias our surface estimations.

For bucket measurements, the main salinity errors arise from improper sealing of water samples, from occasional contamination, from evaporation effect during the sampling carried out from a 20- to 30-m-high bridge, and from salinometer error. The accuracy of bucket SSS measurements is thus difficult to evaluate. An estimate can be made by comparing bucket SSS, collected so as to approximate SOP situations, with SSS derived from almost-simultaneous CTD measurements. This was done during two SURTROPAC (Survey of Tropical Pacific) research cruises in the western tropical Pacific [*DuPenhoat et al.*, 1990; *Delcroix et al.*, 1991]. The mean and rms differences between bucket and CTD measurements obtained from these cruises were 0.088 and 0.10, respectively. Interestingly, a similar mean difference (0.064) was found between the *Levitus* [1982] climatological mean SSS sampled along the four mean shipping routes and our long-term mean SSS calculated over a different period. As compared with a CTD datum, a raw bucket SSS measurement thus appears slightly overestimated by 0.06–0.09 with an accuracy of about ±0.1. Compared with this, salinometer error (0.003) and changes in the salinity of samples stored for 1–3 months (mean increase of 0.003) were found to be negligible.

Because of the multiple processing stages applied to the

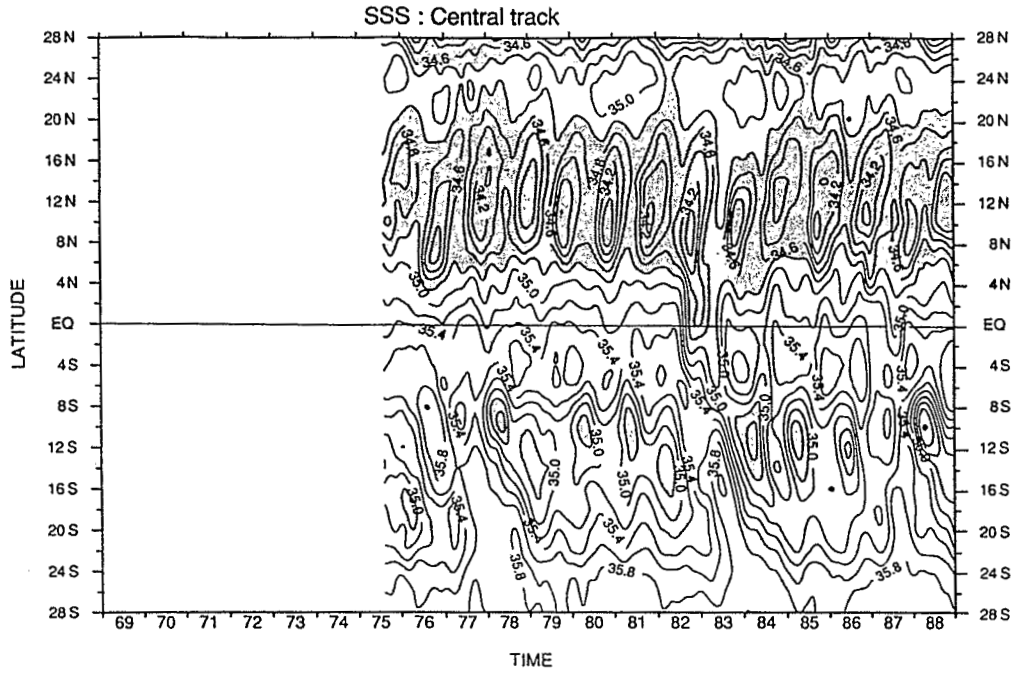

Fig. 3. Time-latitude diagram of sea surface salinity for the central track. Contour intervals are 0.2, and shaded areas denote sea surface salinity below 34.8.

raw SSS data, precision in the gridded SSS field is not easy to determine. On a mean, a gridded SSS value represents 6.1 bucket samples which were collected during a given month, within a 2° latitude by 10°–15° longitude band. Since more measurements give a more reliable mean, the rms error of a gridded value is reduced roughly by a factor of $6.1^{1/2}$. However, precision in a gridded value may still be biased by inadequate time-space sampling.

In the time domain, sampling effects upon monthly mean calculations can be estimated by subsampling continuous salinity time series at a given location. In the tropical Pacific, continuous series are available at 0°–140°W and 0°–165°E [see *McPhaden et al.*, 1990], where near-surface salinity was recorded every 15–30 min from November 1987 to November 1988 at 11m depth and from November 1988 to May 1990 at 26 m depth, respectively. For each location, "true" monthly means were calculated from the continuous time series and then compared with monthly means estimated

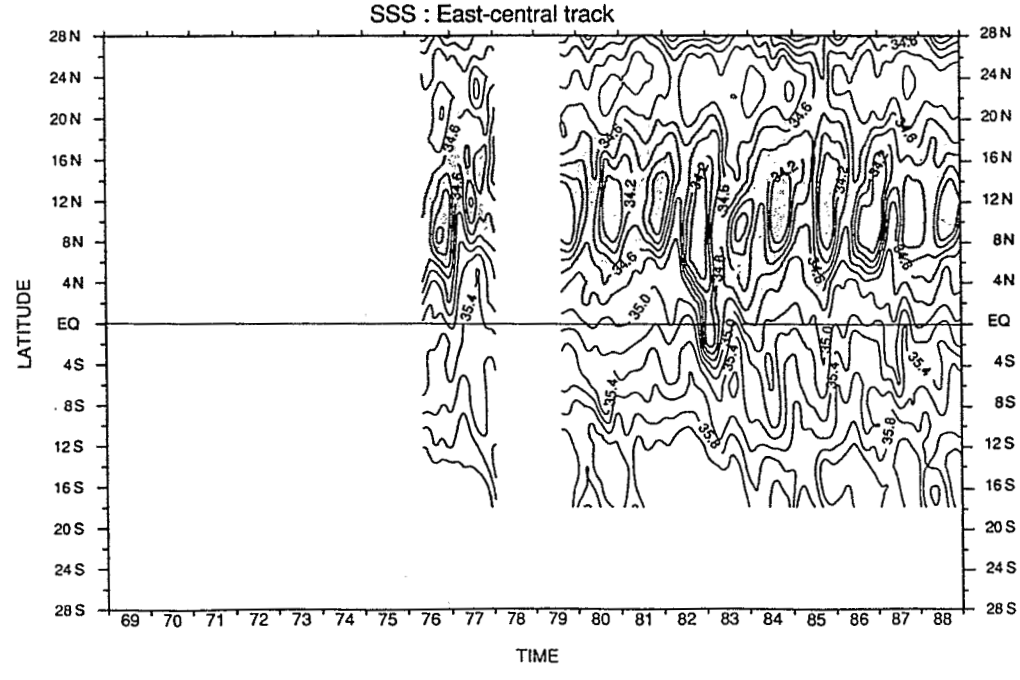

Fig. 4. Time-latitude diagram of sea surface salinity for the east central track. Contour intervals are 0.2, and shaded areas denote sea surface salinity below 34.8.

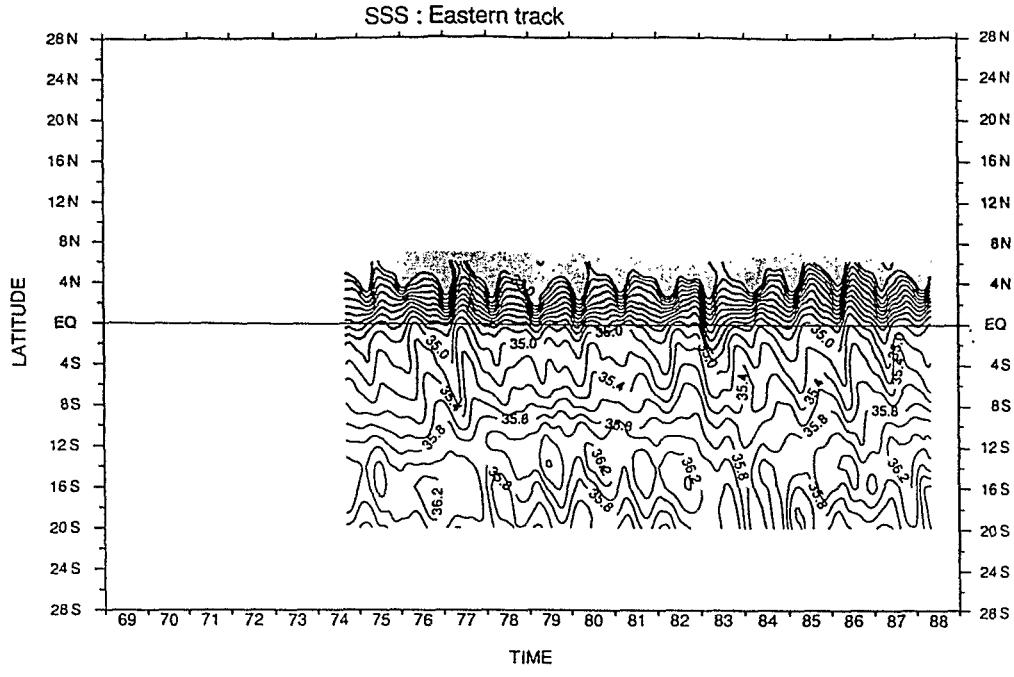

Fig. 5. Time-latitude diagram of sea surface salinity for the eastern track. Contour intervals are 0.2, and shaded areas denote sea surface salinity below 34.8.

from data extracted at the dates of bucket measurements obtained for the closest tracks (2.7 observations per month over the considered periods). The mean and rms differences between 26 "true" and estimated monthly mean values were −0.0007 and 0.09, respectively. Note that the rms value is in agreement with a subsampling experiment based on bucket measurements along the central track during 1979–1985 [*Kessler et al.*, 1985].

Sampling tests were also performed in the space domain. For this purpose, we used near-surface salinity data recorded every 5 min along a single track during a SURTROPAC cruise (Figure 6). With data from this cruise, we compared "true" 2° latitude averaged salinities calculated from the 5-min resolution, with 2° latitude averaged salinities estimated from 3- to 6-hour sampling intervals that approximate SOP data. In this case, the mean and rms differences between "true" and estimated values were −0.01 and 0.03–0.05, respectively. Hence sampling effects in the time-space domain would not bias our monthly estimations too much. It is worth noting, however, that a notable salinity front, as observed at 1°S in Figure 6, cannot be fully resolved from sporadic bucket measurements.

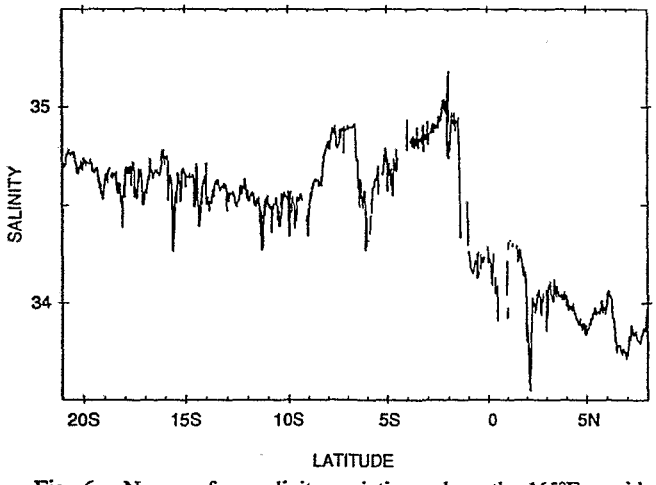

Fig. 6. Near-surface salinity variations along the 165°E meridian. Measurements were made from December 14 to 27, 1989, with an STD 12 Applied System instrument, recording salinity data every 5 min at 2–3 m depth.

Finally, estimating the errors associated with grouping the scattered SSS data into mean tracks is not an easy problem. So far, this can be done neither from observations, in the absence of simultaneous zonally separated SSS measurements, nor from model simulations, in which SSS changes are poorly reproduced. Future moored arrays along the equator [*Hayes et al.*, 1991], as well as the expected improvement of model capability in simulating SSS changes, will make such error estimates possible. In conclusion, there is no stringent way of estimating the precision in the gridded SSS values. We estimated some potential errors for specific time periods and locations, and not strictly for surface measurements. Given the order of magnitude of these errors, we believe that the overall accuracy of the gridded SSS fields is probably better than 0.1.

Complementary data, including surface wind stress and rainfall, will be further utilized. Surface wind stress has been derived from pseudostress (units of $m^2\ s^{-2}$) data kindly provided by the Florida State University (FSU). It consists of monthly mean values onto a 2° latitude by 2° longitude grid mesh [*Goldenberg and O'Brien*, 1981]. A constant drag coefficient $C_d = 1.2 \times 10^{-3}$ was used to convert to stress unit. In addition, island rainfall measurements with long time series were gathered at selected stations situated near the four shipping routes. Monthly precipitation data were obtained from the Service Météorologique National in Nouméa (New Caledonia) and Papeete (Tahiti, French Polynesia).

TABLE 1. Characteristics of Stations Near the Selected Tracks

Station	Latitude	Longitude	Precipitation, mm yr^{-1}	Amplitude, mm	Phase, days	Correlation Coefficient	Period
			Western Track				
Guam	13°33'N	144°50'E	2738	121	231	0.76	1969–1988
Truk	7°22'N	152°01'E	3461	60	220	0.47	1969–1988
Ponape	6°58'N	158°17'E	4638	68	176	0.43	1969–1988
Rabaul	4°13'S	152°11'E	2124	91	20	0.86	1969–1988
Honiara	9°25'S	160°03'E	1991	99	18	0.88	1969–1988
Pekoa	15°31'S	167°08'E	2381	91	30	0.77	1973–1989
Vila	17°44'S	168°19'E	2246	103	38	0.87	1969–1989
Ouanaham	20°45'S	167°13'E	1826	84	32	0.77	1969–1988
Nouméa	22°16'S	166°27'E	1011	39	67	0.82	1969–1988
Norfolk	29°03'S	167°56'E	1286	39	134	0.88	1969–1988
			Central Track				
Washington	4°43'N	160°25'W	2641	111	94	0.89	1927–1974
Fanning	3°51'N	159°22'W	2313	103	94	0.92	1950–1982
Christmas	1°59'N	157°22'W	695	51	91	0.75	1916–1983
Canton	2°46'S	171°43'W	1122	22	100	0.49	1942–1978
Funafuti	8°31'S	179°12'E	3469	73	12	0.53	1975–1978
Puka-Puka	10°53'S	165°49'W	2850	93	353	0.79	1930–1982
Rotuma	12°30'S	177°04'W	3248	44	36	0.50	1975–1989
Hihifo	13°16'S	176°08'W	3387	98	08	0.64	1975–1989
Apia	13°48'S	171°47'W	3124	135	01	0.70	1975–1988
Maopoopo	14°21'S	178°10'W	3337	147	10	0.93	1978–1989
Suva	18°08'S	178°26'W	3037	114	32	0.66	1975–1988
			East Central Track				
Atuona	9°48'S	139°02'W	1674	53	132	0.75	1976–1988
Takaroa	14°29'S	145°02'W	1805	73	350	0.72	1976–1988
Faaa	17°33'S	149°37'W	1856	137	17	0.80	1976–1988
Rarotonga	21°12'S	159°46'W	2100	60	18	0.62	1976–1988
			Eastern Track				
Cristobal	0°54'S	89°36'W	306	34	42	0.71	1974–1988

The annual mean precipitation and the amplitude of the annual harmonic are in millimeters. Phase of the annual harmonic is in Julian days. The correlation coefficient is between monthly mean years and annual cycles reconstituted from annual harmonics.

and from the Monthly Climatic Data for the World (NOAA National Climatic Data Center, Ashville, N. C.). Station characteristics are given in Table 1. Note that when possible, rainfall data were selected for the same time period as for SSS data. As usual when dealing with island rainfall measurements, it should be kept in mind that they may not be representative of the open ocean because of possible orographic effects. These measurements will thus be used as indicative only of mean seasonal cycles built over long time series. They will not be used to quantify month to month variability over a specific time period.

3. Equation for Surface Salinity Changes

Before analyzing the variations of SSS for the four trans-Pacific tracks, it is useful to briefly present and discuss the equation for surface salinity changes in order to clarify future discussions.

The time-averaged turbulent form of the salt conservation equation is

$$\partial S/\partial t + U\partial S/\partial x + V\partial S/\partial y + W\partial S/\partial z + \partial/\partial x\langle u's'\rangle + \partial/\partial y\langle v's'\rangle + \partial/\partial z\langle w's'\rangle = 0 \quad (1)$$

where S is the mean salinity, s' is the deviation from the mean ($s = S + s'$), (U, V, W) are the zonal, meridional and vertical components of the mean velocity vector, and (u', v', w') are the fluctuating components (e.g., $u = U + u'$). Following *Kraus and Turner* [1967] and neglecting horizontal mixing, (1) is integrated over the depth (h) of the upper mixed-layer salinity to obtain

$$h(\partial S/\partial t + U\partial S/\partial x + V\partial S/y) + \langle w's'\rangle_{z=0} - \langle w's'\rangle_{z=h} = 0 \quad (2)$$

with

$$\langle w's'\rangle_{z=0} = (P - E)S \quad (3a)$$

$$\langle w's'\rangle_{z=h} = -dh/dtH(dh/dt)(S - S_{z=h}) \quad (3b)$$

Precipitation and evaporation rates (in meters per second) are denoted by P and E, respectively, and H is the Heaviside unit function (see appendix of *Sui et al.* [1991] for a detailed discussion of (3*b*)). After a rearrangement of (2), from (3*a*) and (3*b*) the local rate of change of mixed-layer salinity is governed by the equation

$$\partial S/\partial t = -U\partial S/\partial x - V\partial S/\partial y + h^{-1}dh/dtH(dh/dt) \cdot (S - S_{z=h}) + h^{-1}(E - P)S \quad (4)$$

Equation (4) expresses that the local rate of change of mixed-layer salinity (left-hand side) results from variations due to the mean zonal (right-hand side, first term) and meridional (second term) salt advection to the rate at which the mixed layer deepens, weighted by a vertical salinity

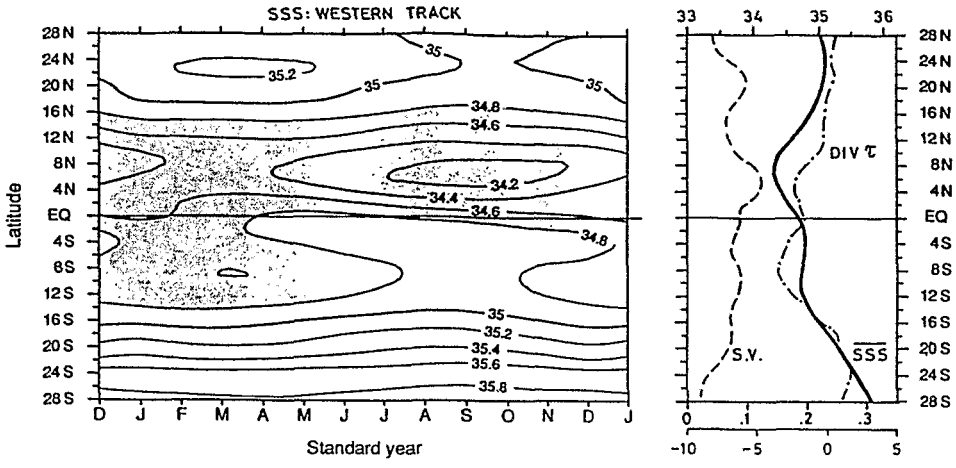

Fig. 7. (Left) Mean seasonal cycle of sea surface salinity for the western track. Contour intervals are 0.2, and shaded areas denote sea surface salinity below 34.8. (Right) Mean sea surface salinity (SSS bar, heavy line, top scale), mean wind stress divergence (div τ, dash-dotted line, bottom scale -10 to 5×10^{-8} N m^{-3}), and amplitude of the seasonal SSS variations (S.V, dashed line, bottom scale 0 to 0.35) along the western track.

gradient (third term), and to the balance between evaporation and precipitation rates, weighted by mixed-layer depth (last term). Given the multiple processes involved in (4), it is clearly difficult to quantify the relative contributions of the sources of salinity variations using observations. As a consequence, while the left-hand side of (4) can be analyzed, it should be kept in mind that the right-hand side will be discussed only qualitatively throughout the paper. It should, however, provide a useful guideline for future works involving quantitative estimates. Specific treatments of (4) will be utilized in sections 4 and 5.

In section 4, the mean SSS distribution is analyzed along each track. There the contributions of precipitation as well as the effect of horizontal salt advections are discussed. Following *Stommel* [1965], the horizontal velocity (U, V) is broken down into Ekman wind drift components (U_e, V_e) and geostrophic components (U_g, V_g). The terms $[(U_e + U_g)\ \partial S/\partial x]$ and $[(V_e + V_g)\ \partial S/\partial y]$ in (4) are roughly estimated from the FSU wind data set ($U_e = \tau_y/\rho fh$; $V_e = -\tau_x/\rho fh$), and from SSS and 0/1000 dbar dynamic height anomalies derived from *Levitus* [1982] climatological data, and sampled every 2° latitude along each track, and 10°W and 10°E of each track. Owing to the equatorial singularity in the computations of Ekman and geostrophic currents, salt advections are not calculated within the region 2°N to 2°S.

In section 5 a simplification of (4) is used to compare the annual variations of SSS and P. Following *Hires and Montgomery* [1972], if variations of SSS are only governed by a simple periodic variations in P given by

$$P = A_p \cos(\omega t - \theta) \tag{5}$$

then, to the first order, time integration of (4) gives

$$S = S_0 - A_s \sin(\omega t - \theta) \tag{6}$$

where ω is the annual frequency and $A_s = A_p S_0 (\omega h)^{-1}$ is the amplitude of the annual salinity variation. In this case, it is clear from (5) and (6) that the minimum in salinity would occur a quarter cycle, i.e., 3 months, after the maximum in P. (Note that a similar conclusion could be drawn if P were replaced by a given advection term). Such a situation is tested in section 5 on P and SSS data sets.

Finally, it is worth mentioning that the mean vertical advection of salt is not included in (4), reflecting the fact that the advective term $W\partial S/\partial z$ becomes zero within the mixed layer (and $W = 0$ at the surface). An important consequence is that equatorial upwelling cannot contribute directly to SSS variations. However, the effect of upwelling is indirect through its modification of the salinity immediately below the mixed-layer $S_{z=h}$. In other words, the small-scale turbulence flux of salt, as reflected in the third term on the right-hand side of (4), is likely to have a significant effect on the large-scale equatorial SSS distribution. This turbulence flux is hard to quantify.

4. Mean Sea Surface Salinity

As a first step, we determined the magnitudes of the along-track mean SSS before analyzing the seasonal and interannual variabilities. The mean SSS were computed from the gridded monthly values excluding the 1972–1973, 1976, 1982–1983, and 1987 El Niño–Southern Oscillation (ENSO) years as defined by *Quinn et al.* [1987]. These ENSO years were removed because they induce a non-Gaussian character in the time variations of SSS. An a posteriori justification is given in section 6. For consistency, the means of wind stress divergence (Figures 7–10, right panels) were derived in a similar way along each track. Note that the mean SSS (Figures 7–10) were calculated over approximately the same period of time (1975–1988), except for the western track where SSS observations started as early as 1969.

Previous studies of SSS distribution over the tropical Pacific [*Reid*, 1969, *Levitus*, 1986] have evidenced two large high-salinity cores centered at about 20°S, 120°W (SSS > 36.0), and 25°N, 170°W (SSS > 35.0). Signatures of these two maxima are perceptible (Figures 7–9) along the western track (24°N), the central track (24°N), and the east central track (24°N and 18°S). The existence of these SSS maxima is generally ascribed to the excess of evaporation over precipitation. Maps of global distribution of $E - P$ for climatological conditions [*Baumgartner and Reichel*, 1975; *Weare et*

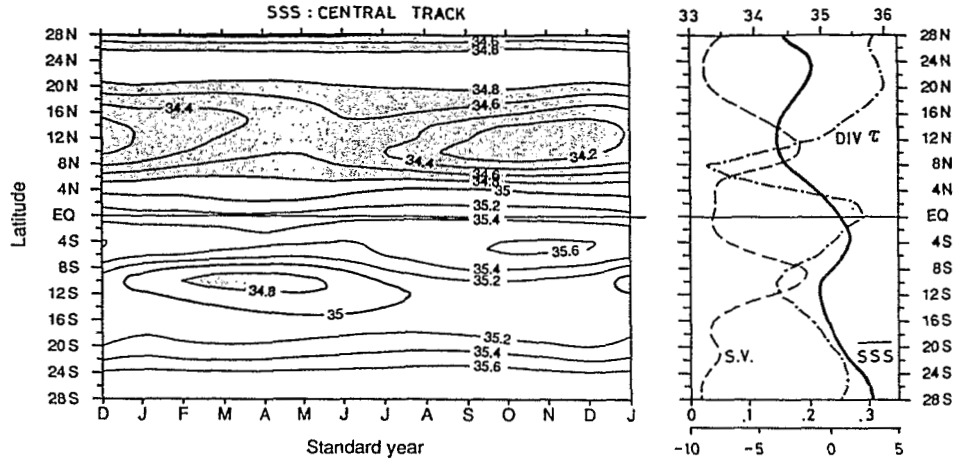

Fig. 8. (Left) Mean seasonal cycle of sea surface salinity for the central track. Contour intervals are 0.2, and shaded areas denote sea surface salinity below 34.8. (Right) Mean sea surface salinity (SSS bar, heavy line, top scale), mean wind stress divergence (div τ, dash-dotted line, bottom scale -10 to 5×10^{-8} N m^{-3}), and amplitude of the seasonal SSS variations (S.V, dashed line, bottom scale 0 to 0.35) along the central track.

al., 1981; *Bryan and Oort*, 1984] show, however, that $E - P$ extrema are 6° to more than 10° farther equatorward than these SSS maxima. Given that estimates by various authors of the climatological mean of $E - P$ can differ even qualitatively from one another, the apparent meridional dislocation between $E - P$ and SSS maxima must be viewed with caution. In addition, salt advection by surface currents might also contribute to some extent to maintaining the SSS maxima (see below).

Large-scale maps of SSS [e.g., *Levitus*, 1986] also portray two low-salinity tongues in the tropical Pacific. These tongues extend roughly from the Indonesian archipelago to French Polynesia, and zonally across most of the basin between 8°N and 14°N. Once again, the signatures of these large-scale features are well reflected in our bucket SSS measurements (Figures 7–10). In the northern hemisphere, from the western to the eastern track, SSS minima appear at 6°–8°N (SSS < 34.3), 10°–12°N (SSS < 34.3), 10°–12°N (SSS < 34.3), and near the Panama coastline (SSS < 32.5). In the southern hemisphere the SSS minima exist only for the western and central tracks, at 8°–10°S (SSS < 34.7), and 10°–12°S (SSS < 35.0), respectively. These SSS minima are located about 2° further poleward than the maxima in surface wind stress convergences (Figures 7–10, right panels) which, in turn, are situated 2° to 4° further poleward than maximum precipitation [see *Riehl*, 1979]. Thus the presence of the SSS minima does not stem only from the precipitation maxima whose positions are 4°–6° closer to the equator. Large-scale maps of mean annual rainfall over the tropical Pacific [*Taylor*, 1973; *Dorman and Bourke*, 1979; *Eliot and Reed*, 1984] confirm that the axes of maximum precipitation associated with the Intertropical Convergence Zone (ITCZ) and the South Pacific Convergence Zone do not exactly coincide with these SSS minima. Hence vertical mixing and/or advection of salt by near-surface currents must be playing a part in the maintenance of these SSS minima. Previous authors suggested that contributions of eastward and/or westward advections are possible in the northern hemisphere where there are low-salinity pools on each side of the Pacific at the latitudes of the SSS minima. The 0/1000 dbar along-track

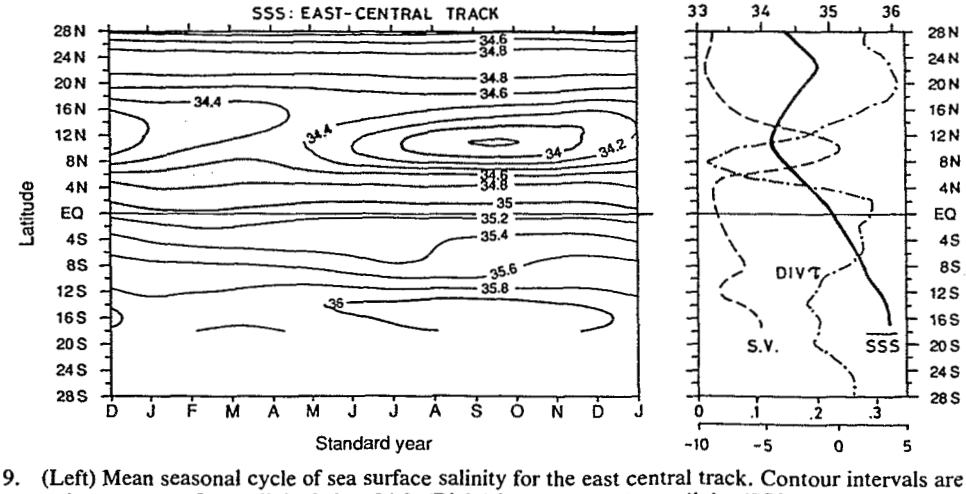

Fig. 9. (Left) Mean seasonal cycle of sea surface salinity for the east central track. Contour intervals are 0.2, and shaded areas denote sea surface salinity below 34.8. (Right) Mean sea surface salinity (SSS bar, heavy line, top scale), mean wind stress divergence (div τ, dash-dotted line, bottom scale -10 to 5×10^{-8} N m^{-3}), and amplitude of the seasonal SSS variations (S.V, dashed line, bottom scale 0 to 0.35) along the east central track.

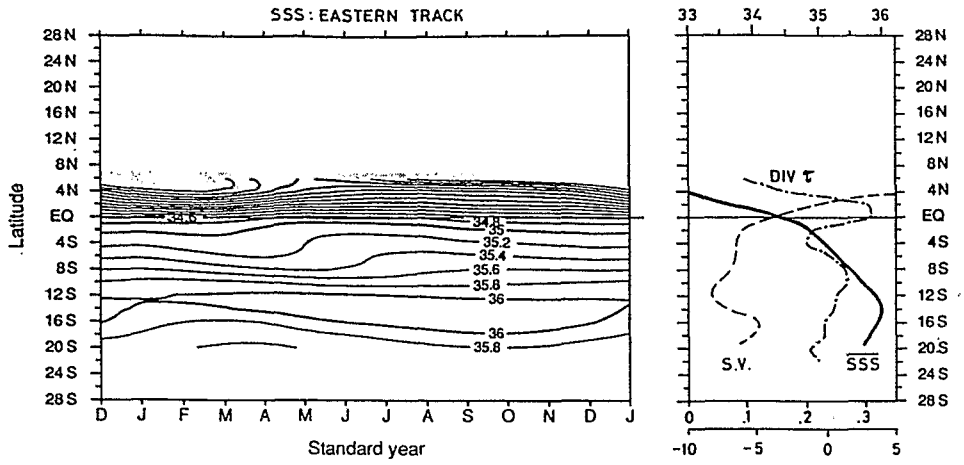

Fig. 10. (Left) Mean seasonal cycle of sea surface salinity for the eastern track. Contour intervals are 0.2, and shaded areas denote sea surface salinity below 34.8. (Right) mean sea surface salinity (SSS bar, heavy line, top scale), mean wind stress divergence (div τ, dash-dotted line, bottom scale -10 to 5×10^{-8} N m^{-3}), and amplitude of the seasonal SSS variations (S.V, dashed line, bottom scale 0 to 0.35) along the eastern track.

dynamic topographies (not shown here), as inferred from the *Levitus* [1982] data set, demonstrate that the SSS minima are not situated in the geostrophic surface current cores (also, compare *Kessler and Taft*'s [1987] Figures 3 and 6). Rather, these minima appear close to surface dynamic height ridges and troughs, indicating near-zero zonal currents and little effect of zonal geostrophic salt advection. As was mentioned in section 3, a rough estimate of Ekman and geostrophic salt advections can be obtained from Levitus' climatological data (used for calculating $\partial S/\partial x$, $\partial S/\partial y$, U_g, and V_g) and from long-term mean FSU wind stress data (used for calculating U_e and V_e). These estimates, derived by assuming a mixed-layer salinity $h = 25$ m, are presented in Figure 11 for the central track; note that to facilitate interpretation in terms of salinity units, the Ekman and geostrophic salt advections are time integrated over $DT = 1$ year. Figure 11 clearly indicates that the meridional salt advections have a greater influence on salinity than the zonal salt advections. Along the central track, the contribution of meridional Ekman salt transport is the dominant factor accounting for salt advections, particularly within 2°–10°N. Over a 1-year period, salt advection by mean surface currents would induce an increase of salinity ranging from about +6 at 2°N to +2 at 10°N. For the purpose of comparison, this is the same order of magnitude as the precipitation effect estimated from the term $h^{-1} PS$ in (4) with the same $h = 25$ m and $P = 3$–5 m yr^{-1} as derived from climatological maps. Between about 2°–4° latitude and the axes of maximum precipitation associated with the ITCZ and SPCZ, i.e., where V_e and $\partial S/\partial y$ are of opposite sign, the meridional Ekman salt transport thus counteracts the effect of rainfall upon SSS changes. Poleward of these axes but still within the heavy rainfall region (>2 m yr^{-1}), salt advection becomes negligible and fails to balance rainfall effect. This might explain why SSS minima are 4°–6° further poleward than rainfall maxima. A similar conclusion was reached for the western and east central tracks. The along-track SSS minima thus appear to be a delicate balance between precipitation and meridional salt avections.

In the equatorial band, relative SSS maxima are found for the western and central tracks at about 2°–4°S. Right at the equator are negative meridional SSS gradients whose magnitudes range from 0.05 to 0.2 per degree of latitude, from

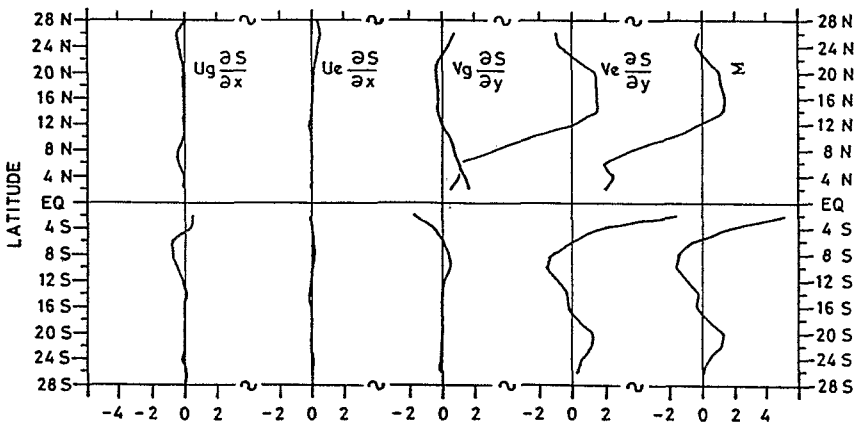

Fig. 11. Estimates along the central track of quantities involved in (4). The right-hand curve (Σ) is the sum of the zonal and meridional geostrophic ($U_g\ \partial S/\partial x$, $V_g\ \partial S/\partial y$) and Ekman ($U_e\ \partial S/\partial x$, $V_e\ \partial S/\partial y$) salt advections. Each quantity is time-integrated over $DT = 1$ year to facilitate interpretation in terms of salinity units. Note that a negative value corresponds to a salinity increase (see (4)).

the western to the eastern tracks. These negative SSS gradients are similar to the subsurface (25–50 m) meridional gradients of salinity [e.g., *Wyrtki and Kilonsky*, 1984], suggesting that vertical mixing may play a key role in determining the near-equatorial SSS distribution.

5. Seasonal Variability

A mean year for SSS was calculated for each track (Figures 7–10, left panels), using the monthly gridded values but omitting the ENSO years as defined in the previous section. The standard deviation of the 12 months from the mean year was used as a measure of the seasonal variability (Figures 7–10; dashed lines on right panels). Along each track, the maximum seasonal variabilities are located 0°–2° closer to the equator than the SSS minima. The maximum variability increases eastward along the ITCZ where it reaches 0.13, 0.19, 0.26, and over 0.38 from the western to the eastern tracks. In the southern hemisphere it culminates for the central track (0.20) in the vicinity of the SPCZ.

Except for the eastern track, the timing of the mean seasonal SSS cycle is quite uniform from track to track. In the vicinity of the ITCZ, minimum SSS values occur in boreal autumn, that is, half a year after the minimum SSS values observed near the SPCZ. In various places of the tropical Pacific, this timing has been thought to be closely related to the local rainfall regimes [*Hires and Montgomery*, 1972; *Donguy and Hénin*, 1975, 1977; *Delcroix and Hénin*, 1989]. Normalized mean seasonal cycles of precipitation (Figure 12) obtained for stations near our selected tracks (see Table 1) were thus used to assess the relationship between P and SSS. For consistency with SSS, the ENSO years were also omitted in computation of the mean P cycles.

In the southern hemisphere the seasonal precipitation maxima (Table 1, Figure 12) occur in January for the stations located under the SPCZ (Rabaul, Honiara, Pekoa, Funafuti, Puka-Puka, Rotuma, and Hihifo). From Table 1 it is clear that these stations present a strong annual mean P (2–3 m yr^{-1}), a well-marked annual P cycle (mean R over 0.7), and a relatively strong annual P amplitude (mean value $A_p = 84$ mm). As is detailed in section 3, if variations of SSS are entirely governed by P, then the minimum SSS would occur 3 months after the maximum P, i.e., in April as observed in Figures 7–8. In addition, the annual P amplitude A_p would induce an annual SSS amplitude $A_s = 0.2$ (see (6)) in agreement with what is found from the actual SSS data. Phase and amplitude between the annual cycles in P and SSS are thus correctly related, and we can conclude that P governs the SSS changes near the selected stations.

On both sides of the SPCZ, to the south at Vila, Ouanaham, Nouméa, and Norfolk and to the north at Atuona and Canton, precipitation maxima occur from February to May, gradually later in the year than the January precipitation maxima under the SPCZ [*Donguy and Hénin*, 1976*a*]. Near these stations, the seasonal SSS variability is quite small, probably reflecting the local weaknesses of the annual P amplitude.

Very few stations exist in the northern hemisphere near our selected tracks. Under the ITCZ, the two available stations (Truk and Ponape) present a strong annual mean P (3–4 m yr^{-1}) with maximum P occurring between June and August, i.e., 2–3 months before the minimum SSS observed close to these stations. The order of magnitude of the annual SSS amplitude $A_s = 0.17$, as expected from (6) with $A_p = 64$ mm (mean value for Truk and Ponape) is similar to that of the observed amplitude. Hence the seasonal SSS cycle is still consistent with the P forcing.

In the northern part of the eastern track there is a very strong seasonal SSS cycle with minimum SSS occurring in February–March. Finding quantitative explanations for this cycle is not a simple task. As was mentioned by *Wyrtki* [1981], the salt budget of the cool tongue representative of the equatorial upwelling is greatly hampered by the strong meridional SSS gradient, and it cannot be rigorously established through a box model study. The following qualitative inspection, however, shows that the phases of possible forcing functions are all consistent with the timing of the observed SSS cycle. Indeed, the minimum SSS is entirely concomitant with peak near-equatorial rainfall associated with the southernmost annual position of the ITCZ [*Hastenrath and Lamb*, 1977] (also, see the P variations for Cristobal in Figure 12). Moreover, the minimum SSS coincides with the February to May reversal period of the SEC [*Halpern*, 1987] which reduces the usual import of higher-salinity water from the region off Peru. Conversely, maximum SSS occurs during the strong wind period (July–September) associated with well-developed SEC and equatorial upwelling, both favoring an increase in SSS through horizontal advection of saltier water and vertical mixing. Increased evaporation during July–September also probably contributes to augment SSS at the equator and south of it, where evaporation may exceed precipitation [*Weare et al.*, 1981]. The observed SSS cycle within the cool tongue thus results from the effects of precipitation, evaporation, and horizontal and vertical salt advections, though it was impossible to quantify the relative importance of each process.

In conclusion, on the basis of scattered precipitation stations, we have confirmed that the seasonal SSS variations in the vicinity of the ITCZ and SPCZ are largely consistent with the seasonal variations of the local rainfall regimes. In the open ocean, future accurate rainfall estimates from satellite data as well as direct rainfall measurements from moorings can be expected to make it possible to comprehensively assess the relationship between the seasonal variations in P and SSS.

The contribution of salt advection on the seasonal SSS variations was not identified here, in the absence of suitable measurements. Although usable in section 3 for analyzing the mean SSS distribution, on a seasonal time scale, the Levitus data indeed present too many data-sparse regions to be used for estimating the different advective terms in (4). The seasonal variations of the meridional Ekman salt transport ($V_e\ \partial S/\partial y$) can, however, be estimated from the FSU wind stress and the actual SSS data. Computations of $V_e\ \partial S/\partial y$ along the central track show that in the convergence zones, minimum (maximum) meridional Ekman transports of saltier water are in phase with maximum (minimal) rainfall. This suggests that $V_e\ \partial S/\partial y$ would reinforce precipitation effect on the seasonal SSS variations. Concerning zonal geostrophic salt advection ($U_g\ \partial S/\partial x$), the North Equatorial Countercurrent and South Equatorial Countercurrent vary seasonally for the western and central tracks, and they are strongest when the SSS is minimum in their respective regions [*Kessler and Taft*, 1987; *Tournier*, 1989], but not 3 months before, as would be required in order to

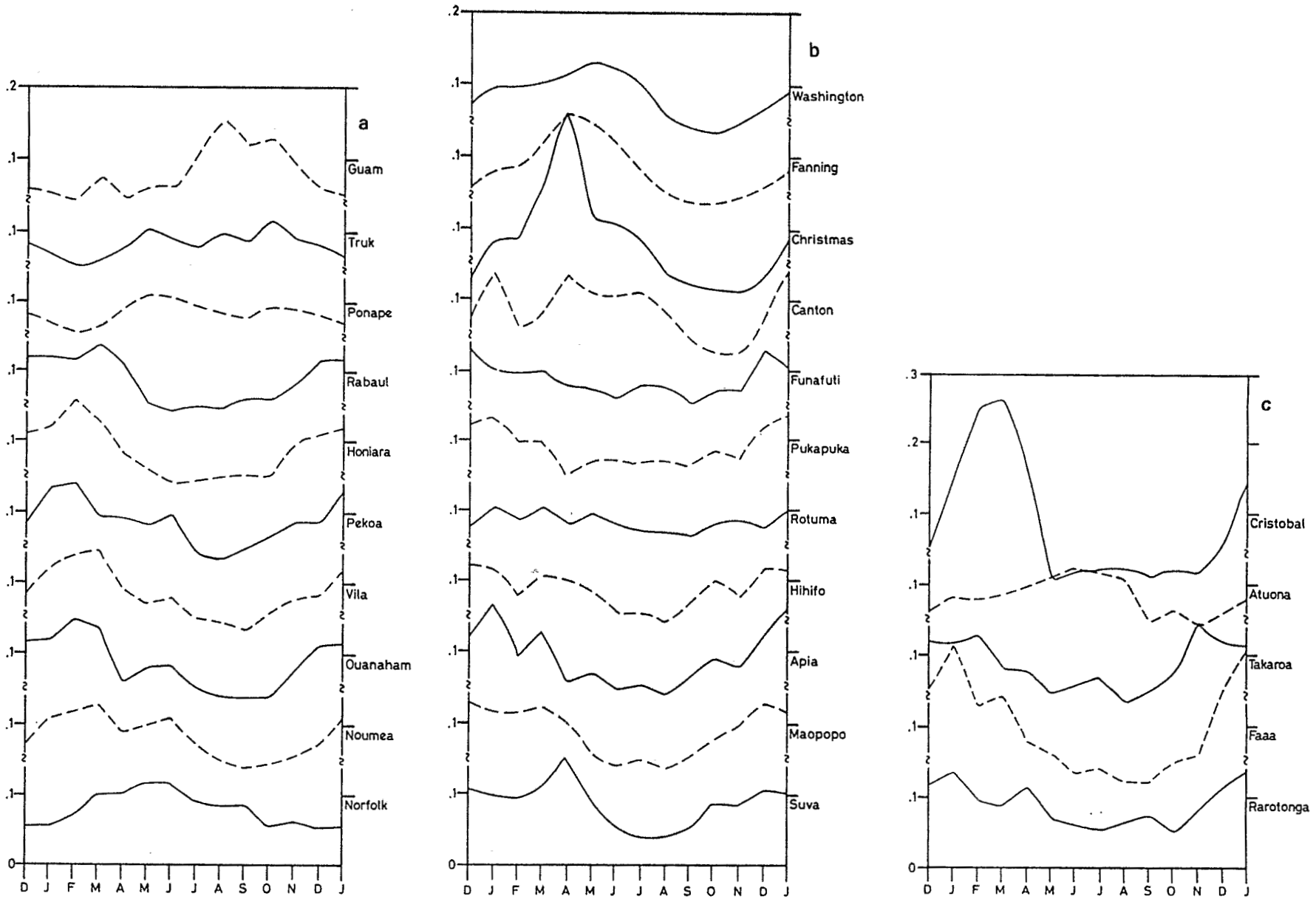

Fig. 12. Mean seasonal cycles of precipitation for stations near the (*a*) western, (*b*) central, and (*c*) east central and eastern tracks. Station characteristics are listed in Table 1. Precipitation values have been normalized by the annual means (i.e., real amount of monthly rainfall are obtained in multiplying the normalized values by the annual mean precipitation values given in Table 1).

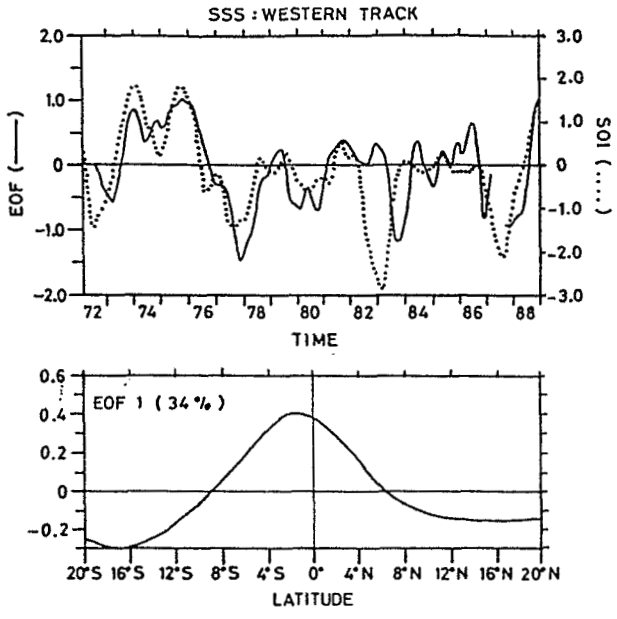

Fig. 13. First empirical orthogonal function (EOF) of sea surface salinity for the western track. The solid lines in the top and bottom panels are the EOF time function and the associated EOF spatial pattern, respectively. A positive product between the time function (left scale) and the spatial pattern represents a positive salinity anomaly. The dotted line in the top panel is the Southern Oscillation index (SOI, right scale) defined as the difference between the standardized sea level pressure anomalies at Tahiti and Darwin (Tahiti minus Darwin). Monthly SOI values are normalized by the mean annual standard deviation, and smoothed with an 11-month Hanning filter.

conclude that these currents govern the seasonal SSS variations (see section 3). Furthermore, estimates of $U_g\ \partial S/\partial x$ demonstrate that this advective term is probably not sufficient to account for SSS changes. For example, at 8°N along the central track, seasonal change in U_g which is about 20 cm s^{-1} [*Kessler and Taft*, 1987, Figure 14] represents a SSS change $\partial S/\partial t$ of about 0.2 per 6 months, i.e., half the observed SSS change (if $\partial S/\partial x$ is assumed to be constant and equal to 0.15 per 20° longitude according to Levitus data). Hence without information on seasonal $\partial S/\partial x$ changes, it cannot be concluded that zonal geostrophic advection plays a part in the seasonal SSS variations. Furthermore, the contributions of evaporation and vertical mixing both remain to be quantified.

6. Interannual Variability

The widely used EOF method [*Kutzbach*, 1967] has been employed to bring out the interannual versus the seasonal SSS variations. The following presents the resulting analysis for each shipping track, now limited to the region between 20°N and 20°S in order to avoid too many data gaps in the corresponding time series.

6.1. *The Western Track*

Along the western track, the spatial patterns and the associated time coefficients of the first three EOFs explain most of the total SSS variance (80%). The first EOF (34% of the variance) is represented in Figure 13. The spatial pattern is roughly a bell-shaped function, with the acme at 2°S, and two zero crossings near 8°S and 6°N. The associated 1972–1988 time function presents a very good correspondence with the Southern Oscillation Index (SOI). Excluding the exceptional 1982–1983 El Niño event, the best correlation of the two time series ($R = 0.83$) is obtained when the EOF time function lags behind the SOI by 2–3 months (from the complete time series; $R = 0.69$ is maximum for 4–5 month time lag). During 1982–1983, the 6- to 7-month time lag between the two time series reflects the unusual way in which the 1982–1983 El Niño evolved [see *Philander*, 1990]. The EOF time function exhibits negative values during five remarkable periods. Each of these periods is associated either with an aborted (1979–1980), moderate (1976–1977 and 1986–1987), strong (1972–1973), or very strong (1982–1983) ENSO phenomenon [*Donguy and Dessier*, 1983; *Quinn et al.*, 1987]. This implies that during an ENSO event, fresher-than-average SSS appears along the western track within ±6°–8° of the equator, with extreme SSS decreases at 2°S latitude. Conversely, saltier-than-average SSS emerges poleward of 6°–8° latitude, with maximum SSS increases for the southern latitudes.

Since the earliest ENSO studies, several analyses have demonstrated the relationships between ENSO and large-scale precipitation patterns [e.g., *Stoeckenius*, 1981; *Rasmusson and Wallace*, 1983; *Ropelewski and Halpert*, 1987]. The following suggests that explanations for the ENSO-related SSS signals along the western track can be found in these relationships. *Ropelewski and Halpert* [1987] built a composite ENSO precipitation cycle, and identified regions of the globe that have strong ENSO-related precipitation signals (see their Figure 2). When the western SOP track is superimposed on these regions, a fair agreement is observed between the locations of ENSO-related increased precipitation and the locations of ENSO-related decreased SSS, and vice versa. In conclusion, ENSO-related SSS changes along the western track appear to be governed by ENSO-related precipitation changes. Using an ENSO precipitation composite to draw such a conclusion is necessarily restrictive. For example, the composite does not include the 1982–1983 and 1986–1987 ENSO. However, the regions with strong *P*-ENSO relationships were those influenced during these last two events [*Quiroz*, 1983; *Chen*, 1983; *Ropelewski*, 1984; *Bergman*, 1984; *Morlière and Rébert*, 1986; *Ardanuy et al.*, 1987; *Janoviak and Arkin*, 1991]. Furthermore, in the analysis of *Ropelewski and Halpert* [1987], the lack of near-equatorial stations near the western track raises doubt as to whether or not our ENSO-related extreme SSS changes at 2°S coincide with strong ENSO-related precipitation. Nevertheless, recent analyses of satellite rainfall estimates for the 1982–1983 and 1986–1987 ENSO [*Ardanuy et al.*, 1987; *Janoviak and Arkin*, 1991] demonstrate that maximum rainfall anomalies are located near 2°S and, as such, give credence to our conclusion.

Obviously, this conclusion is very much at the mercy of the available data and should thus be somewhat tempered. First, as was observed for the 1986–1987 ENSO period (T. Delcroix et al., Variation of the western tropical Pacific Ocean, 1986–1988, submitted to *Journal of Geophysical Research*, 1991), the ability of advective processes to influence the salinity field cannot be dismissed. For example, equatorward Ekman surface currents associated with westerly winds occurring during ENSO events probably influence SSS near the equator. Second, we cannot as yet assess whether the ENSO-related precipitation changes are large

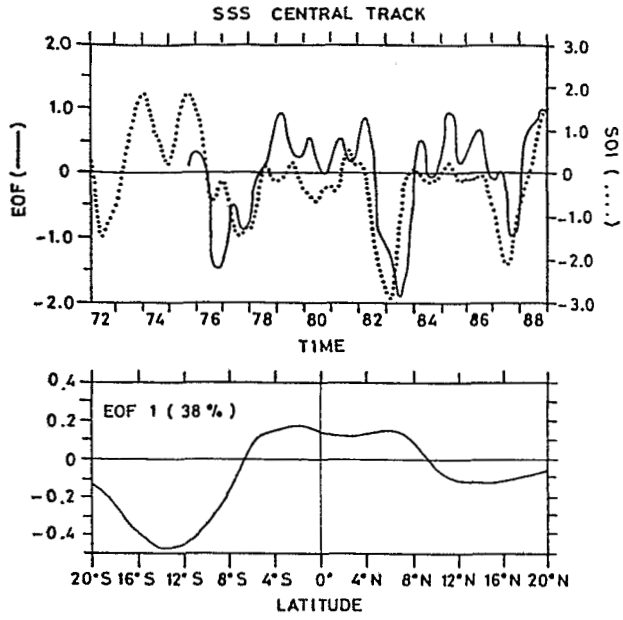

Fig. 14. First empirical orthogonal function (EOF) of sea surface salinity for the central track. The solid lines in the top and bottom panels are the EOF time function and the associated EOF spatial pattern, respectively. A positive product between the time function (left scale) and the spatial pattern represents a positive salinity anomaly. The dotted line in the top panel is the Southern Oscillation index (SOI, right scale) defined as the difference between the standardized sea level pressure anomalies at Tahiti and Darwin (Tahiti minus Darwin). Monthly SOI values are normalized by the mean annual standard deviation, and smoothed with an 11-month Hanning filter.

enough to explain the associated SSS variations. Indeed, we do not have enough information on the depth of mixed-layer salinity, and quantitative open-ocean rainfall estimates, as deduced from stations or from satellite techniques, are often unreliable [*Arkin and Ardanuy*, 1989]. Finally, the utilization of a composite ENSO cycle precipitation, built over a specific time period, prohibits a careful investigation of phase differences between P and SSS variations linked to ENSO. The remarkable coincidence in location between ENSO-related precipitation and SSS changes in the western tropical Pacific should thus be refined in order to be made more explicit.

The second and third EOF of SSS along the western track (not shown here) explain 24% and 21% of the total variance, respectively. The two spatial patterns have their peak amplitude in opposite hemispheres. In agreement with the previous section, the two associated time functions reveal a 6-month time lag between the annual SSS cycle in the ITCZ mean area (minimum SSS in September–October) and the one in the SPCZ mean area (minimum SSS in March–April).

6.2. *The Central Track*

The spatial patterns and the associated 1975–1988 time coefficients of the first EOF (38% of the variance) are shown in Figure 14 for the central track. As for the western track, the 1976–1977, 1982–1983, and 1986–1987 ENSO signals are all extracted by the first EOF time function, which is highly correlated with the SOI; the best correlation of the two time series (R = 0.65) occurs when the EOF time function lags behind the SOI by 2–3 months. The associated spatial pattern still separates the 8°N to 8°S equatorial band from the two regions of opposite sign covering the remaining northern and southern parts of the track. During ENSO periods, this indicates coherent fresher-than-usual SSS between 8°N and 8°S, and saltier-than-usual SSS poleward of 8°, especially in the SPCZ mean area. Our results thus confirm and expand the results obtained on specific areas for the 1982–1983 ENSO [*Delcroix and Gautier*, 1987; *Kessler and Taft*, 1987; *Delcroix and Hénin*, 1989].

Explanations for these ENSO-related SSS changes can further be grounded on the existing links between ENSO and large-scale precipitation patterns. Looking along the central track, the regions of ENSO-related enhanced precipitation (10°N to 10°S) and notable rainfall shortage (10°S–24°S), as subjectively determined by *Ropelewski and Halpert* [1987], are once again in agreement with the regions we found for decreased and increased SSS. The agreement near the equator is now more plausible than for the western track owing to the existence of near-equatorial rainfall stations near the central track. Also, numerous studies have revealed increased ENSO-related precipitation in the vicinity of the equator from the date line to about 150°W and decreased ENSO-related precipitation in the SPCZ mean area [*Horel and Wallace*, 1981; *Rasmusson and Carpenter*, 1982; *Sadler and Kilonsky*, 1983; *Ardanuy et al.*, 1987; *Janoviak and Arkin*, 1991]. Hence it is reasonable to expect that, during ENSO periods, rainfall excess and deficit play a major role in governing the SSS field along the central track.

As was noted before, such an explanation is subject to a minimum of caution because a causative analysis of SSS variability would require knowledge of several processes. For example, *Delcroix and Hénin* [1989] have demonstrated that mixing and advection together have probably the same order of magnitude as the effect of reduced rainfall upon the 1982–1983 SSS changes in the SPCZ mean area. The possible effects of salt advection by the surface currents can also be suspected. Observed reversals of the South Equatorial Current (SEC) [e.g., *Firing et al.*, 1983], usually flowing from regions of higher SSS, probably contribute to decreasing the near-equatorial SSS in 1982–1983. *Kessler and Taft* [1987] estimated, however, that the advective term $U\ \partial S/\partial x$ is not quite enough to account for the 1982–1983 drop in equatorial SSS in the central Pacific.

The second and third EOF of SSS along the central track (not shown here) respectively account for 23% and 14% of the total variance. The space functions are more heavily weighted near 8°–10°S (second EOF) and 8°–10°N (third EOF), and the associated space functions are 6 months out of phase one from the other. As was detailed in section 5, these EOFs represent the seasonal SSS variations associated with the rainfall activities of the SPCZ (second EOF; minimum SSS in March–April) and ITCZ (third EOF; minimum SSS in October–November).

6.3. *The East Central Track*

As a cautionary note, it must be recalled that the east central track presents the shortest SSS time series (1976–1978 + 1980–1988) and also has a sampling rate 2 to 4 times less than for other tracks.

Along the east central track, the first three EOF (not shown here) explain three quarters of the total variance. The first EOF (37%) identifies a seasonal SSS cycle which is

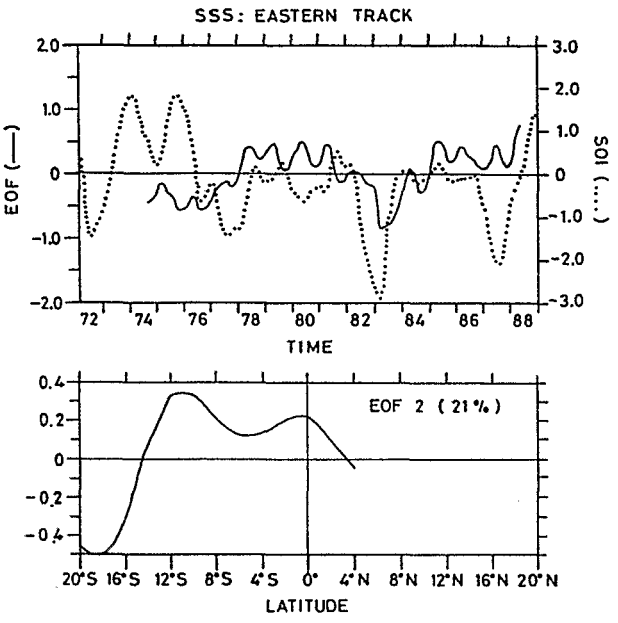

Fig. 15. Second empirical orthogonal function (EOF) of sea surface salinity for the eastern track. The solid lines in the upper and bottom panels are the EOF time function and the associated EOF spatial pattern, respectively. A positive product between the time function (left scale) and the spatial pattern represents a positive salinity anomaly. The dotted line in the top panel is the Southern Oscillation index (SOI, right scale) defined as the difference between the standardized sea level pressure anomalies at Tahiti and Darwin (Tahiti minus Darwin). Monthly SOI values are normalized by the mean annual standard deviation, and smoothed with an 11-month Hanning filter.

more heavily weighted within 8°–12°N, in the ITCZ mean area (minimum SSS in September–October). The second EOF (20%) still shows a distinctive seasonal SSS cycle with coherent variations south of 4°N (minimum SSS in March–April). Details of these cycles are given in section 5. The third EOF (16%) characterizes the extremely strong 1982–1983 ENSO episode with fresher-than-average SSS between 8°N and 6°S and peak value at 4°–6°N.

Unlike for the western and central tracks, the strongest SSS variability here is thus no longer associated with ENSO events. A similar conclusion will be drawn for the eastern track, indicating that ENSO-related SSS changes mainly involve the western part of the tropical Pacific. This is in marked contrast with what has been found for the sea surface temperature field [e.g., *Weare*, 1982].

6.4. *The Eastern Track*

Along the eastern track, the first two EOFs of SSS explain two thirds of the total variance. The first EOF space function (not shown here) depicts increasing positive values from 8°S to 4°N, i.e., mostly within the tongue of cool water distinctive of the equatorial upwelling. The associated time function illustrates a well-marked annual SSS cycle, with nearly constant amplitude and minimum SSS in February–March. Tentative explanations for this annual cycle were been given in the preceding section.

The second EOF of SSS for the eastern track (Figure 15) accounts for 21% of the total variance. The time function is not correlated with the SOI, although it separates the 1976–1977 and 1982–1983 ENSO from the remaining time series, including the 1986–1987 phenomenon. The associated space function indicates maximum SSS decreases at the equator and within 8°–12°S. As was discussed by *Donguy and Hénin* [1980], such SSS variations might reflect weaker-than-usual horizontal and vertical advections of salty water and increased rainfall associated with the southward shift of the ITCZ. The oceanic and meteorological events observed during the 1982–1983 ENSO [*Hayes et al.*, 1986; *Sadler and Kilonsky*, 1983] do not conflict with their interpretation. South of 14°S (note that the eastern track is as far west as 140°W at 14°S). *Delcroix and Hénin* [1989] have demonstrated that the augmentation of SSS results mainly from the equatorward shift of the SPCZ. The lack of ENSO-related SSS signals in 1986–1987 suggests that a moderate El Nino is not sufficient to affect the SSS field along the eastern track.

7. CONCLUSIONS

As detailed in the introduction, salinity is a prominent parameter in many oceanic studies, and its surface distribution may condition and/or reflect mass and heat exchanges between the ocean and the atmosphere. Because of their importance, sea surface salinity variations are being monitored for the three tropical oceans, through an ORSTOM ship-of-opportunity program that started as early as 1969. This paper has focused upon the data yielded by this program for the tropical Pacific ocean only, over the period 1969–1988. Specifically, four well-sampled shipping tracks were selected (Figure 1) in order to describe and analyze the along-track mean SSS distributions, together with the SSS changes at seasonal and interannual time scales.

Along each track, the mean SSS distribution evidenced SSS minima which are located 4°–6° degrees farther poleward than the axes of maximum precipitation associated with the ITCZ and SPCZ. Order-of-magnitude estimates of salt advections suggested that this meridional dislocation between rainfall maximum and SSS minimum mainly reflects the effect of meridional Ekman salt transport. On a seasonal time scale and in the ITCZ and SPCZ regions, timing and amplitude of the rainfall regime were found to be sufficient to account for the local SSS changes.

The most interesting findings were the interannual SSS changes found to be strongly related with the SOI in the western half of the tropical Pacific. During each studied ENSO period, well-marked SSS decreases appear between about 8°N and 8°S, only for the tracks located west of 150°W. Conversely, SSS increases arise poleward of 8° latitude, particularly in the SPCZ mean area. These SSS changes are in qualitative agreement with what would be expected if they were governed only by ENSO-related precipitation changes. Indeed, ENSO periods are known to be characterized by a major displacement of the ascending branch of the Walker and Hadley cells which induces an eastward shift of the equatorial flood region from Indonesia to the central Pacific, and by notable rainfall deficits on both sides of the equatorial belt [*Barnett*, 1984; *Ardanuy et al.*, 1987; *Ropelewski and Halpert*, 1987]. Regions in the western and central tropical Pacific with strong ENSO-related precipitation signals thus correspond to regions where we have observed consistent ENSO-related SSS changes. Obviously, the lack of precise open-ocean rainfall measurements, the paucity of rainfall station networks, and our present inability to quantify changes in the mixed-layer salinity and depth as well as the

exact contributions of horizontal and vertical salt advections prevented us from being more categorical in our conclusions.

In view of the strong relationships between precipitation and SSS changes, an interesting perspective would be to utilize SSS monitoring in conjunction with satellite-derived precipitation data to improve rainfall estimates in the tropics. Methods should be developed to adequately combine meteorological and oceanic rainfall-related parameters in order to achieve a better mapping and thus a better climatic interpretation of rainfall changes. In this context, bucket SSS measurements based on the existing ship-of-opportunity networks should be systematically replaced by continuous along-track SSS measurements which greatly improve the precision and the spatial resolution of SSS (see Figure 6).

Another relevant perspective would be to use the present along-track SSS time series, and then the future fine-scale measurements, as "ground truth" for model output. Indeed, even sophisticated models [e.g., *Harrison et al.*, 1989] at present fail to hindcast SSS variability, probably because they ignore changes due to surface water fluxes which, as shown here, seem to constitute the main forcing function for SSS. Simply reproducing the present along-track SSS changes at seasonal and interannual time scales would thus be a very stringent test for model capability.

Finally, it is worth recalling that information of the kind we have contributed for surface salinity is still very scarce for subsurface salinity. To the author's knowledge, the variability of subsurface salinity can be determined only in specific regions of the tropical Pacific and at best on a seasonal time scale [*Wyrtki and Kilonsky*, 1984; *McPhaden et al.*, 1990]. Such a gap in the knowledge of the tropical oceans is likely to be detrimental to climate modeling efforts, especially when we consider the potential role of salinity in the dynamics and thermodynamics of the western Pacific warm pool [cf. *Lukas*, 1990]. Multiyear measurements of upper ocean salinity such as are now gradually becoming available at mooring locations in the equatorial Pacific can thus be expected to greatly improve our knowledge of the tropical ocean variability.

Acknowledgments. We are most thankful to the officers and crews of numerous merchant and navy ships which voluntarily participate in the surface ship-of-opportunity program. The present analysis represents the combined efforts of many ORSTOM researchers and technicians, and in particular owes much to J. R. Donguy's insight and tenacity in initiating and continuing the ship-of-opportunity program, despite inevitable difficulties. Other data sets were supplied by M. McPhaden (moored near-surface salinity time series), J. O'Brien (FSU wind field), the Service Météorologique National in New Caledonia and French Polynesia (precipitation), the U.S. Department of Commerce (precipitation), and the Climate Analysis Center in Washington, D. C. (Southern Oscillation Index). Programming support was mainly provided by F. Masia, while M. Sicard, P. Waigna, and R. Gérard carefully analyzed and/or managed most of the bucket samples. The comments of R. Lukas and an anonymous reviewer were helpful in improving the manuscript. M. Laplagne gave pertinent editing suggestions. All these contributions are gratefully acknowledged.

REFERENCES

Ardanuy, P. E., P. Cuddapah, and H. L. Kyle, Remote sensing of water convergence, deep convection, and precipitation over the tropical Pacific ocean during the 1982–1983 El Niño. *J. Geophys. Res.*, *92*(C13), 14,204–14,216, 1987.

Arkin, P. A., and P. E. Ardanuy, Estimating climatic-scale precipitation from space: A review, *J. Clim.*, *2*, 1229–1238, 1989.

Barnett, T. P., Interaction of the monsoon and Pacific trade wind system at interannual time scales, III, A partial anatomy of the southern oscillation, *Mon. Weather Rev.*, *112*, 2388–2400, 1984.

Baumgartner, A., and E. Reichel, *The World Water Balance*, Elsevier, New York, 1975.

Bergmann, K. H., The climate of autumn 1983—Featuring the conclusion of a major El Niño event, *Mon. Weather Rev.*, *112*, 1441–1456, 1984.

Bryan, F., High-latitude salinity effects and interhemispheric thermohaline circulation, *Nature*, *323*, 301–304, 1986.

Bryan, F., and A. Oort, Seasonal variations of the global water balance based on aerological data, *J. Geophys. Res.*, *89*(D7), 11,717–11,730, 1984.

Chen, W. Y., The climate of spring 1983—A season with persistent global scale anomalies associated with El Niño, *Mon. Weather Rev.*, *111*, 2363–2384, 1983.

Cooper, N. S., The effect of salinity on tropical ocean models, *J. Phys. Oceanogr.*, *18*, 697–707, 1988.

Delcroix, T., and C. Gautier, Estimates of heat content variations from sea level measurements in the central and western tropical Pacific from 1979 to 1985, *J. Phys. Oceanogr.*, *17*, 725–734, 1987.

Delcroix, T., and C. Hénin, Mechanisms of subsurface thermal structure and sea surface thermohaline variabilities in the southwestern tropical Pacific during 1979–85, *J. Mar. Res.*, *47*, 777–812, 1989.

Delcroix, T., and F. Masia, Atlas des variations de température et de salinité de surface du Pacifique tropical (1969–1988), Rapports scientifiques et techniques, *Sci. de la Mer, Oceanogr. Phys.*, *2*, 151 pp., Centre ORSTOM de Nouméa, Nouméa, New Caledonia, 1989.

Delcroix, T., F. Gallois, F. Masia, and P. Waigna, Rapport de la campagne SURTROPAC 14 à bord du N.O. *Le Noroit* (13 mars au 8 avril 1991), Rapports de mission, *Sci. de la Mer, Oceanogr. Phys.*, *4*, 117 pp., Centre ORSTOM de Nouméa, Nouméa, New Caledonia, 1991.

Donguy, J. R., Recent advances in the knowledge of the climatic variations in the tropical Pacific ocean, *Prog. Oceanogr.*, *19*, 49–85, 1987.

Donguy, J. R., and A. Dessier, El Niño–like events observed in the tropical Pacific, *Mon. Weather Rev.*, *111*, 2136–2139, 1983.

Donguy, J. R., and C. Hénin, Surface waters in the north of the Coral Sea, *Aust. J. Mar. Freshw. Res.*, *26*, 293–296, 1975.

Donguy, J. R., and C. Hénin, Relations entre les précipitations et la salinité de surface dans l'océan Pacifique tropical sud-ouest basées sur un échantillonnage de surface de 1956 à 1973, *Ann. Hydrog.*, *4*, 53–59, 1976*a*.

Donguy, J. R., and C. Hénin, Anomalous navifacial salinities in the tropical Pacific Ocean, *J. Mar. Res.*, *34*, 355–364, 1976*b*.

Donguy, J. R., and C. Hénin, Navifacial conditions in the northwest Pacific ocean, *J. Oceanogr. Soc. Jpn.*, *33*, 183–189, 1977.

Donguy, J. R., and C. Hénin, Surface salinity fluctuations between 1956 and 1973 in the western South Pacific Ocean, *J. Phys. Oceanogr.*, *8*, 1132–1134, 1978.

Donguy, J. R., and C. Hénin, Surface conditions in the eastern equatorial Pacific related to the intertropical convergence zone of the winds, *Deep Sea Res.*, *27*, 693–714, 1980.

Dorman, C. E., and R. H. Bourke, Precipitation over the Pacific Ocean, 30°S to 60°N, *Mon. Weather Rev.*, *107*, 896–910, 1979.

DuPenhoat, Y, F. Gallois, M. J. Langlade, G. Reverdin, and H. Walico, Rapport de la campagne SURTROPAC 13 à bord du N.O. *Le Suroit* (1 au 28 décembre 1989), Rapports de mission, *Sér. Sci. de la Mer Oceanogr. Phys. 3*, 167 pp., Centre ORSTOM de Nouméa, Nouméa, New Caledonia, 1990.

Eliot, W. P., and R. K. Reed, A climatological estimate of precipitation for the world ocean, *J. Clim. Appl. Meteorol.*, *23*, 434–439, 1984.

Firing, E., R. Lukas, J. Sadler, and K. Wyrtki, Equatorial undercurrent disappears during 1982–1983 El Niño, *Science*, *222*, 1121–1123, 1983.

Goldenberg, S., and J. J. O'Brien, Time and space variability of tropical Pacific wind stress, *Mon. Weather Rev.*, *109*, 1190–1207, 1981.

Halpern, D., Observations of annual and El Niño thermal and flow

variations at 0°, 110°W and 0°, 95°W during 1980–1985, *J. Geophys. Res.*, *92*(C8), 8197–8212, 1987.
Harrison, D. E., W. S. Kessler, and B. S. Giese, Ocean circulation model hindcasts of the 1982–83 El Niño: Thermal variability along the ship-of-opportunity tracks, *J. Phys. Oceanogr.*, *19*, 397–418, 1989.
Hastenrath, S., and P. J. Lamb, *Climate Atlas of the Tropical Atlantic and Eastern Pacific Oceans*, 97 charts, University of Wisconsin Press, Madison, 1977.
Hayes, S., L. J. Mangum, R. T. Barber, A. Huyer, and R. L. Smith, Hydrographic variability west of the Galapagos Islands during the 1982–83 El Nino, *Prog. Oceanogr.*, *17*, 137–162, 1986.
Hayes, S., L. J. Mangum, J. Picaut, A. Sumi, and K. Takeuchi, TOGA-TAO: A moored array for real-time measurements in the tropical Pacific ocean, *Bull. Am. Meteorol. Soc.*, *72*(3), 339–347, 1991.
Hires, R. I., and R. B. Montgomery, Navifacial temperature and salinity along the track from Samoa to Hawaii, 1957–1965, *J. Mar. Res.*, *30*, 177–200, 1972.
Horel, J. D., and J. M. Wallace, Planetary-scale phenomenon associated with the Southern Oscillation, *Mon. Weather Rev.*, *109*, 813–829, 1981.
Janoviak, J. E., and P. A. Arkin, Rainfall variations in the tropics during 1986–1989, as estimated from observations of cloud-top temperature, *J. Geophys. Res.*, *96*, suppl., 3359–3374, 1991.
Kessler, W. S., and B. A. Taft, Dynamic heights and zonal geostrophic transports in the central tropical Pacific during 1979–84, *J. Phys. Oceanogr.*, *17*, 97–122, 1987.
Kessler, W. S., B. A. Taft, and M. McPhaden, An assessment of the XBT sampling network in the central Pacific, *US TOGA 4*, Univ. Corp. for Atmos. Res., Boulder, Colo., 1985.
Kraus, E., and J. Turner, A one-dimensional model of the seasonal thermocline, II, The general theory and its consequences, *Tellus*, *19*, 98–106, 1967.
Kutzbach, J. E., Empirical eigenvectors of sea-level pressure, surface temperature and precipitation complexes over North America, *J. Appl. Meteorol.*, *6*, 791–812, 1967.
Lazier, J. R., Seasonal variability of temperature and salinity in the Labrador Current, *J. Mar. Res.*, *40*, 341–356, 1982.
Levitus, S., Climatological atlas of the world ocean, *NOAA Prof. Pap. 13*, 173 pp., U.S. Govt. Print. Off., Washington. D. C., 1982.
Levitus, S., Annual cycle of salinity and salt storage in the world ocean, *J. Phys. Oceanogr.*, *16*, 322–343, 1986.
Lukas, R., The role of salinity in the dynamics and thermodynamics of the western Pacific warm pool, International TOGA Scientific Conference, Proceedings, *Rep. WCRP-43*, pp. 73–83, World Clim. Res. Prog., World Meteorol. Organ., Geneva, 1990.
Lukas, R., and E. Lindstrom, The mixed layer of the western equatorial Pacific Ocean, *J. Geophys. Res.*, *96*, suppl., 3343–3358, 1991.
McPhaden, M., H. P. Freitag, and A. J. Shepherd, Moored salinity time series measurements at 0°, 140°W, *J. Atmos. Oceanic Technol.*, *7*, 568–575, 1990.
Miller, J., The salinity effect in a mixed layer ocean model, *J. Phys. Oceanogr.*, *6*, 29–35, 1976.
Morlière, A., and J. P. Rébert, Rainfall shortage and El Niño Southern Oscillation in New Caledonia, southwestern Pacific, *Mon. Weather Rev.*, *114*, 1131–1137, 1986.
Neumann, G., Seasonal salinity variations in the upper strata of the western tropical Atlantic ocean, I, Sea surface salinities, *Deep Sea Res.*, *16*, 165–177, 1969.
Philander, S. G., *El Niño, La Niña, and the Southern Oscillation*, 293 pp., Academic, San Diego, Calif., 1990.
Quinn, W., V. Neal, and S. Antunez de Mayolo, El Niño occurrences over the past four and a half centuries, *J. Geophys. Res.*, *92*(C13), 14,449–14,461, 1987.
Quiroz, R. S., The climate of the El Niño winter of 1982–83—A season of extraordinary climatic anomalies, *Mon. Weather Rev.*, *111*, 1685–1706, 1983.
Rasmusson, E. M., and T. Carpenter, Variations in tropical sea surface temperature and surface wind fields associated with the Southern Oscillation/El Niño, *Mon. Weather Rev.*, *110*, 354–384, 1982.
Rasmusson, E. M., and J. M. Wallace, Meteorological aspects of the El Niño/Southern Oscillation, *Science*, *222*, 1195–1202, 1983.
Reid, J. L., Sea-surface temperature, salinity, and density of the Pacific Ocean in summer and in winter, *Deep Sea Res.*, *16*, 215–224, 1969.
Riehl, H., *Climate and Weather in the Tropics*, 611 pp., Academic, San Diego, Calif., 1979.
Ropelewski, C. F., The climate of summer 1983—A season of contrast and extremes, *Mon. Weather Rev.*, *112*, 591–609, 1984.
Ropelewski, C. F., and M. S. Halpert, Global and regional scale precipitation patterns associated with the El Niño/Southern Oscillation, *Mon. Weather Rev.*, *115*, 1606–1626, 1987.
Sadler, J. C., and B. J. Kilonsky, Meteorological events in the central Pacific during 1983 associated with the 1982–83 El Niño, *Trop. Ocean Atmos. Newsl. 21*, pp. 3–5, Joint Inst. for the Study of Atmos. and Ocean, Univ. of Wash., Seattle, 1983.
Saur, J. F., Surface salinity and temperature on the San Francisco–Honolulu route June 1966–December 1970 and January 1972–December 1975, *J. Phys. Oceanogr.*, *10*, 1669–1680, 1980.
Stoeckenius, T., Interannual variations of tropical precipitation patterns, *Mon. Weather Rev.*, *109*, 1233–1247, 1981.
Stommel, H., *The Gulf Stream, A Physical and Dynamical Description*, 248 pp., University of California Press, Berkeley, 1965.
Sui, C. H., K. M. Lau, and A. K. Betts, An equilibrium model for the coupled ocean-atmosphere boundary layer in the tropics, *J. Geophys. Res.*, *96*, suppl., 3151–3164, 1991.
Sverdrup, H. U., M. W. Johnson, and R. Fleming, *The Oceans: Their Physics, Chemistry, and General biology*, Prentice-Hall, Englewood Cliffs, N. J., 1942.
Taylor, R. C., An atlas of Pacific island rainfall, *Rep. HIG 73-8*, 165 pp., Hawaii Inst. of Geophys., Univ. of Hawaii, Honolulu, 1973.
Tournier, R., Variabilité de la structure thermique et des courants à l'ouest et au centre de l'océan Pacifique tropical, Thèse de doctorat, 154 pp., Univ. Paris VI, Paris, 1989.
Weare, B. C., El Niño and tropical Pacific Ocean surface temperatures, *J. Phys. Oceanogr.*, *12*, 17–27, 1982.
Weare, B. C., P. T. Strub, and M. D. Samuel, Annual mean surface heat fluxes in the tropical Pacific Ocean, *J. Phys. Oceanogr.*, *11*, 705–717, 1981.
Wyrtki, K., An estimate of equatorial upwelling in the Pacific, *J. Phys. Oceanogr.*, *11*, 1205–1214, 1981.
Wyrtki, K., and B. Kilonsky, Mean water and current structure during the Hawaii-to-Tahiti shuttle experiment, *J. Phys. Oceanogr.*, *14*, 242–254, 1984.

T. Delcroix and C. Hénin, Groupe SURTROPAC, ORSTOM, B.P. A5, Nouméa, New Caledonia.

(Received March 25, 1991;
accepted June 3, 1991.)